

Cite this: DOI: 10.1039/c1lc20019d

www.rsc.org/loc

PAPER

## Microfluidic chemostat and turbidostat with flow rate, oxygen, and temperature control for dynamic continuous culture†

Kevin S. Lee,<sup>a</sup> Paolo Boccazzi,<sup>b</sup> Anthony J. Sinskey<sup>b</sup> and Rajeev J. Ram<sup>\*a</sup>

Received 10th January 2011, Accepted 7th March 2011

DOI: 10.1039/c1lc20019d

This work reports on an instrument capable of supporting automated microscale continuous culture experiments. The instrument consists of a plastic-PDMS device capable of continuous flow without volume drift or evaporation. We apply direct computer controlled machining and chemical bonding fabrication for production of fluidic devices with a 1 mL working volume, high oxygen transfer rate ( $k_L a \approx 0.025 \text{ s}^{-1}$ ), fast mixing (2 s), accurate flow control ( $\pm 18 \text{ nL}$ ), and closed loop control over temperature, cell density, dissolved oxygen, and pH. Integrated peristaltic pumps and valves provide control over input concentrations and allow the system to perform different types of cell culture on a single device, such as batch, chemostat, and turbidostat continuous cultures. Continuous cultures are demonstrated without contamination for 3 weeks in a single device and both steady state and dynamically controlled conditions are possible.

### Introduction

Understanding cell behavior is essential in microbial physiology, genetics, ecology and biotechnology. Growth kinetics, or the relationship between cell growth rate and nutrient supply, plays a vital role in the understanding of cell function. While research has been focused on understanding growth kinetics from a genomic level, there is still great difficulty in making the leap from genetic analysis to accurate verification with controlled cell growth experiments, or cell cultures. Most culture systems operate as batch cultures, providing a fixed amount of nutrients and oxygenation for the initial cells and supporting cell growth until it becomes limited by either a nutrient source or oxygen. Batch cultures are not ideal for characterizing cellular processes since cells are constantly subjected to environmental changes such as changes in acidity, oxygen content, or even increased cell population. It was recognized that in order to study bacterial growth with precision, a constant and controllable environment was necessary. The simultaneous development of the chemostat, a method to grow cells with a continuous nutrient supply by Monod<sup>1</sup> and Novick and Szilard<sup>2</sup> was the first step towards developing reliable continuous culture experiments to study growth kinetics.

Continuous culture under steady state conditions provides results that are much less sensitive to operator variation and lead to more reproducible microarray data, however, operation of continuous culture systems is more complicated.<sup>3</sup> The major difficulties are the need to continuously supply medium and maintain a sterile environment. Unlike batch culture where growth time scales are hours to days, continuous cultures can run for days or weeks at steady state. For long experiments, the cost of medium and maintaining sterility during medium addition become increasingly important and volumes of 500 L per culture are not reasonable.

Microfluidics offers a way to address the difficulties relating to conventional continuous culture systems. A microscale system can run for long periods of time consuming much less media, on the order of 10 mL to 1 L rather than 500 L. In addition, technologies have been developed for microscale bioreactors which address issues regarding environmental sensing and control, mainly through the integration of electrical or optical transducers for measuring oxygen, pH, cell density, and different forms of microscale pumps and mixers for injecting and distributing fluids such as medium components, acid, and base buffers.<sup>4</sup> Integrating all of these microfluidic components into a working continuous culture system can provide a sophisticated level of control not available in conventional systems as well as provide for inexpensive parallelism which would be highly beneficial for long continuous culture experiments.

To date, four micro-chemostat systems utilizing many of the above mentioned microfluidic components have been reported. Balagadde *et al.*<sup>5</sup> developed a micro-chemostat in polydimethylsiloxane (PDMS) in a 16 nL volume. Steady state was demonstrated by direct cell counts, and semi-continuous flow was enabled through valves integrated using

<sup>a</sup>Research Laboratory of Electronics, Massachusetts Institute of Technology, 77 Massachusetts Ave, Cambridge, MA, 02139, USA. E-mail: rajeev@mit.edu

<sup>b</sup>Department of Biology and Health Sciences and Technology, 77 Massachusetts Ave, Cambridge, MA, 02139, USA. E-mail: asinskey@mit.edu

† Electronic supplementary information (ESI) available. See DOI: 10.1039/c1lc20019d

**Table 1** Summary of previous microfluidic continuous culture reactors and their capabilities for environmental control

Type	Reference	$k_1/a/s^{-1}$	Working volume/mL	Parallelism	Control	Analysis	Comments
<i>Continuous microbioreactors</i>							
Circular micro-channel	Balagadde <i>et al.</i> <sup>5</sup>	N.R.	$16 \times 10^{-6}$	6	T, OD, flow	Imaging	No environmental monitoring, no sampling
Perfusion chemostat	Groisman <i>et al.</i> <sup>9</sup>	N.R.	$50 \times 10^{-6}$	1	T	Imaging	No environmental monitoring, no sampling
Stirred membrane aeration	Zhang <i>et al.</i> <sup>6</sup>	0.04	0.150	1	T	DO, pH, OD, sample	No environmental control, no automated flow control
Diffusive removal	Luo <i>et al.</i> <sup>7</sup>	N.R.	$1 \times 10^{-6}$	1	T, OD, flow	Imaging	No environmental monitoring, no sampling, indirect cell removal
Flow through	Edlich <i>et al.</i> <sup>8</sup>	0.004	$8 \times 10^{-3}$	2	T, Flow	OD, DO, sample	No environmental control, no pH monitoring
Integrated mixing, input, and flow control	This report	0.016	1	1	T, DO, OD, flow	DO, pH, OD, sample	Integrated environmental control, integrated flow control

polydimethylsiloxane (PDMS) fabrication processes. However, general PDMS soft lithography based valve integration also resulted in small culture volumes, making it difficult to integrate commercial dissolved oxygen and pH sensors required for environmentally defined steady states. Small volumes also increased surface fouling issues, requiring novel procedures for periodic lysing and cleaning, and prevented offline sampling for chemical analysis. Integration of environmental sensors has also been reported by a micro-chemostat developed by Zhang *et al.*<sup>6</sup> on a larger 150  $\mu\text{L}$  scale. The larger chip volume enabled both the integration of optical sensing techniques and the possibility of offline chemical analysis. Reduced surface fouling issues also enabled passive fouling prevention through surface coatings. Unfortunately, it required moving to rigid plastics to accommodate the increased volume. Without PDMS to plastic bonding technology, PDMS was integrated mechanically to provide aeration, but valve integration was not possible, preventing automated flow, pH, and dissolved oxygen (DO) control. Two other examples have also been recently published. Luo *et al.*<sup>7</sup> developed a nanolitre scale turbidostat but again had no control over environmental parameters likely due to the inability to integrate chemical sensors into nanolitre sized PDMS valve microfluidics. In addition, cell removal was performed diffusively with no direct connection between the growth chamber and waste lines. Edlich *et al.* developed a larger scale system with a volume of 8  $\mu\text{L}$ <sup>8</sup> with measurements of dissolved oxygen and optical density. However, mixing was performed diffusively, resulting in biofilm growth rather than suspension growth, and oxygen transfer rates were low. This larger volume device again did not integrate PDMS valves for control. Other microsystems have also been developed for addressing continuous culture and a comparison of these systems is given in Table 1.

While recently developed microscale continuous reactors address many of the problems of conventional continuous reactors, namely measurement systems and media usage, microscale continuous reactors still require unique solutions to many continuous culture specific problems such as total biomass control and sterility. Biomass control, when implemented, required complicated image processing of microscope images.<sup>5,7</sup> Sterility was only possible through a variety of innovative

methods such as direct heating,<sup>6</sup> periodic lysing,<sup>5</sup> agarose diffusion filtering,<sup>7</sup> and direct 0.22  $\mu\text{m}$  filtering.<sup>8</sup> Without these innovative methods, the smaller continuous cultures exhibited prominent wall growth<sup>5,7-9</sup> and possible back growth to the carbon source.<sup>6</sup>

Since chemostats are frequently used to study cell metabolic rates, sampling of growth chamber fluid for offline analysis is essential to measure chemical products. While microscale cultures reduce cost by reducing media usage, volume reduction also directly affects sampling time negatively. For example, a typical 50  $\mu\text{L}$  sample volume for HPLC taken from a 100 nL bioreactor requires 500 turnovers of the chip volume. For a bacteria cell with a  $1 \text{ h}^{-1}$  growth rate, a single sample can take 500 hours. A summary of the specific volumes for previous continuous microreactors is also presented in Table 1.

All recent advances in microscale continuous reactors have been aimed at developing chemostats, but as mentioned by Flegr<sup>10</sup> there are other continuous modes such as the turbidostat which are equally important. Situations where cells need to be studied in steady state under very high cell densities, non-nutrient limited environments, or under dynamically controllable environmental conditions are not possible with chemostat systems since they rely on a constant flow of media to gradually reach steady state. Many examples exist where turbidostats are necessary, such as directed evolution,<sup>11</sup> microbial photosynthesis,<sup>12-14</sup> and overflow metabolism.<sup>15</sup> While there have been some examples of turbidostat operation, very coarse (16 section<sup>5</sup>) or probabilistic<sup>7</sup> flow control resulted in large variations in cell number around the average density.

In contrast to existing microscale continuous culture systems, by using a recently developed microfabrication process combining plastics and PDMS<sup>16</sup> we have combined the flow control possible with PDMS microfluidics with microlitre to millilitre sized devices enabling online and offline measurement strategies such as optical sensors and HPLC. Coupling active PDMS valves to rigid plastics enables precise control of PDMS membrane deformation, necessary to translate small scale active valves to large volume systems. The reactor integrates multiple fluid inputs and outputs with an on-chip peristaltic pump and oxygenating peristaltic mixer to enable fluid control, oxygen

control, and rapid mixing. Rigid plastic enables accurate optical density measurements, closed loop control over cell density, and consistent volumes. Rigid plastics are necessary to guarantee volume consistency across variations in hydraulic pressure, and also enable methods of evaporation compensation necessary to minimize steady state concentration offsets. Integrated pressure regulation is also possible to prevent flow rate drift. Fabricating the device out of plastic also enables integrated external fluid interfaces, improving reliability and sterility between the device and external components.

## Device design

The continuous culture device with a 1 mL working volume is presented in Fig. 1. Specific device dimensions are given in the ESI†. The following component descriptions are organized from input to output. Eight inputs for fluids are located at the top of the chip for different media and are connected to 35  $\mu$ L on-chip reservoirs to reduce pressure variations. A single peristaltic pump with an injection volume of 210 nL is connected between all 8 reservoirs and the growth chamber. Three interconnected growth chamber sections containing PDMS membranes can be inflated to 500  $\mu$ L per chamber. With a designed volume of 1 mL, only two sections are full, allowing compliance for mixing. Two outputs are provided to enable automatic switching between sample collection and waste output. The connection between the peristaltic pump and outputs is called the pass-through channel. This 25  $\mu$ L microfluidic channel is also connected in series with the mixer to allow mixing of newly injected media with the growth chamber contents.

### Peristaltic mixer

The growth chamber also functions as a peristaltic mixer and is composed of the three growth wells, each with symmetrically rounded 250  $\mu$ L top and bottom halves split by a PDMS membrane. These wells act as valves and can deflect from their equilibrium position to inflate and fill with liquid, or deflate to remove liquid. Active (A) actuation of the three membranes in a circular pattern results in mixing through the interconnected channel. A mixing pattern of {PPO, POP, OPP}, where (P) indicates pressurized and (O) indicates open and vented. The pressurization state is changed every 333 ms during growth.

### Peristaltic pump

Fluid injections are mediated by 8 separate 35  $\mu$ L on-chip reservoirs and a single peristaltic pump with a nominal injection volume of 220 nL. The peristaltic pump consists of 3 valves,<sup>17</sup> which can move discrete plugs of fluid if actuated in the pattern {POP, POO, PPO, OPP, OOP}. The ceiling of the peristaltic pump center valve is designed to nearly equal the volume of the final valve, reducing the backward step typical of peristaltic pumps.

### On-chip reservoir isolation

Blocking valves exist to enable fluid pressurization as well as prevent diffusion between different fluid sections of the device. The external fluid inputs are isolated from the on-chip reservoirs by individual blocking valves (B1). These valves mediate filling of

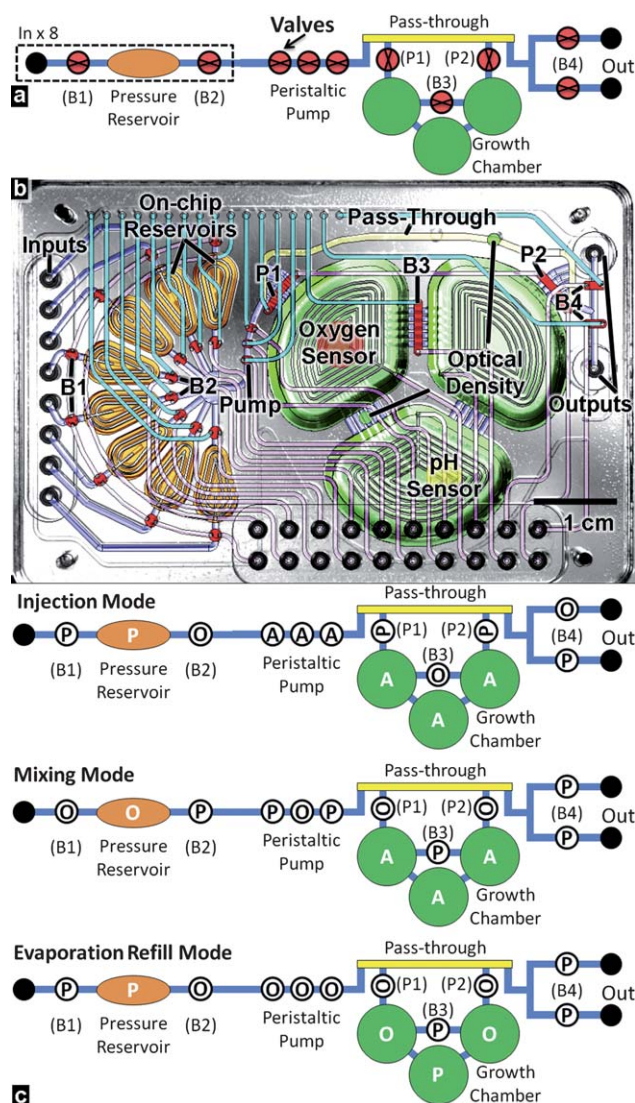


**Fig. 1** (a) Top view schematic of the fluid layer of the microfluidic device from one input to the 2 outputs. 8 inputs are connected to individual on-chip reservoirs through blocking valves (B1). The reservoirs are connected to a peristaltic pump and each reservoir is addressed through another set of blocking valves (B2). A pass-through channel controls the fluid connection between the pump, growth chamber, and outputs through blocking valves (P1 and P2) which block the growth chamber and two output valves (B4). A blocking valve (B3) selects for mixing through the growth chamber and mixing through the pass-through. (b) False color photograph of the continuous culture device with device components and valves labelled in accordance to the schematic in (a). (c) Three operation modes for continuous culture are described. Valve configurations are designated as P closed/pressurized, O open/vented, and A for actively switched on/off. Injection mode is used when fluid input and output are desired. This replaces the fluid in the pass-through channel with new media. Mixing mode then mixes the newly injected pass-through contents with the rest of the growth chamber. Evaporation refill mode uses the on-chip water reservoir to inflate the growth chamber back to full volume.

the on-chip reservoir. The on-chip reservoirs are also isolated from the peristaltic pump by individual blocking valves (B2). These prevent diffusion between different inputs and also allow for pump input selection.

## Pass-through channel

The growth chamber has a variable volume due to the elasticity of the PDMS membrane which is required for peristaltic mixing and valving. As a result, fluid pumped into the growth chamber can accumulate, changing the growth chamber volume. In addition, since the growth chamber is peristaltically mixed, it is under constant pressure resulting in complete removal of the growth chamber contents if a direct output connection is allowed. To mediate volume changes due to the peristaltic pump and growth chamber pressure, an additional constant volume microfluidic channel designated a pass-through channel is introduced connecting the peristaltic pump directly to the output. As shown in Fig. 1(a), the peristaltic pump and output are connected through two paths, one going through the growth chamber, and one going through the pass-through. Two additional valves (P1 and P2) are located at the input and output of the growth chamber which allows for selection of the fluid path to include or exclude the growth chamber. One blocking valve (B3) is also located between two growth chamber sections to force circular flow between the growth chamber and the pass-through. In addition, a blocking valve (B4) is placed before the output. The configuration of the pass-through maintains the growth chamber volume but also necessitates multiple operation modes for the device to function.

## Materials and methods

### Device operation

To maintain the growth chamber volume while still providing integrated peristaltic mixing and flow control requires multiple operation steps mediated by the pass-through channel. Three configurations exist as shown in Fig. 1(c), injection mode, mixing mode, and evaporation refill mode. In general, the chip is placed into either injection or mixing configurations depending on whether a pumping cycle needs to be initiated. At pre-programmed times, evaporation refill mode is initiated to return the chamber to full volume.

**Injection mode.** Fluid injection from a single input is performed by a specific valve configuration. The external input is closed ( $B1 = P$ ), the on-chip reservoirs are pressurized, and one reservoir is connected to the peristaltic pump ( $B2 = O$ ). This allows the pressure from the on-chip reservoir to drive the peristaltic pump. The growth chamber is then disconnected from the rest of the device ( $P1 = P$  and  $P2 = P$ ) and the pass-through channel is directly connected to the output ( $B4 = O$ ). Growth chamber mixing is still enabled by opening the second mixer valve ( $B3 = O$ ). In this configuration, peristaltic pump injections result in new fluid entering the pass-through channel while forcing old growth chamber fluid out of the device. This allows extraction of the growth chamber fluid as long as the newly injected volume is less than the total pass-through channel volume and also ensures that the input and output flow rates are identical.

**Mixing mode.** Once injection into the pass-through has been completed the chip is switched to mixing mode. The peristaltic pump is turned off and blocked, the output is closed ( $B4 = P$ ), and the on-chip reservoir connections are closed ( $B2 = P$ ). After

closing the input and output valves, connecting the growth chamber to the pass-through channel ( $P1 = O$  and  $P2 = O$ ) while closing the second mixer valve ( $B3 = P$ ) forces the mixer to circulate through the pass-through, mixing the new fluid contents with the growth chamber fluid. In addition, opening the external input blocking valve ( $B1 = O$ ) allows the on-chip reservoir to refill through the external input fluid, setting up the on-chip reservoir for the next injection.

**Evaporation refill mode.** The growth chamber mixer is turned off and only one section is pressurized as illustrated in Fig. 1(c). This forces the growth chamber liquid into the two unpressurized sections. If there is any evaporation, the membranes will not inflate fully in the unpressurized chambers. After setting the growth chamber to the proper state, the external inputs are closed ( $B1 = P$ ), the on-chip reservoir is pressurized, and the DI water input valve is connected to the peristaltic pump ( $B2 = O$ ). All three peristaltic pump valves are then opened, allowing a direct connection between the pressurized on-chip reservoir and the growth chamber. The pressurized water from the reservoir reinflates the unpressurized mixer sections until the membranes are fixed against the rigid chamber wall, returning the volume to 1 mL. It is important to maintain the on-chip reservoir pressure to be less than the growth chamber membrane pressure to allow for the DI water flow to stop when the two unpressurized sections are full. After evaporation compensation, the device is again placed into mixing mode.

### Device fabrication

The continuous culture microdevices are fabricated out of polycarbonate (PC) and polydimethylsiloxane (PDMS). Microchannels and features are machined into polycarbonate using a CNC milling machine (Minitech Minimill 4) with various sized balls, squares, drills, and keyseat end mills. After machining, devices are polished using methylene chloride vapor<sup>18</sup> to remove tooling marks and increase the optical clarity. To remove the absorbed solvent, the parts are then annealed at 130 °C in a convection oven.

After polishing device layers, devices are etched in 3 M sodium hydroxide solution and rinsed in isopropanol to activate the surface. Then a chemical adhesive (bis-*n*-isopropoxy-*m*-methoxy-silyl-propylamine) is applied to the surface with a wiper to introduce silicon dioxide groups at the surface.<sup>16</sup> After baking at 65 °C in high humidity to harden the coating, a 65 μm thick PDMS membrane is corona treated for 30 seconds using a corona treater (Electrotech Products BD-20AC) and bonded to the coated PC device. For layers without temperature sensitive components such as optical sensors, parts are subjected to a second thermal anneal at 130 °C to accelerate bonding. For fluid layers, optical sensors are secured in the base of the fluid chamber using double-sided silicone adhesive tape AR-clad 7876.

PDMS membranes are fabricated by spin coating PDMS onto an anti-static polyester transparency (Polymex PR172). Thicknesses are monitored online using an optical coherence interferometer.<sup>19</sup> After coating the transparency with the desired thickness of PDMS, the PDMS film is baked at 65 °C for 4 hours.

The coating and bonding process is then repeated with subsequent layers to form multilayer stacks of PC-PDMS-PC.

Due to the tacky nature of the initial bond, finger pressure is enough to initiate bonding making hydraulic presses and vices unnecessary for the bonding process. After bonding, the two layer device is baked at 50 °C for 4 hours or left at room temperature overnight. For passive fluid and gas layers, silicone adhesive tape is used instead of chemical adhesive to reduce fabrication complexity. A full layer stack including four polycarbonate layers, one PDMS valving membrane, and two silicone adhesive layers is provided in the ESI† along with fabrication steps.

Finally, the internal surfaces of the devices are modified with PEG following a modified procedure by Zhang *et al.*<sup>6</sup> Internal surfaces are first coated with a 5% aqueous solution of aminoethyl-amino-propyl-silanetriol (Gelest Inc.) for 12 hours at room temperature. After rinsing with DI water, the device is coated with a copolymer of polyethylene glycol (PEG) and polyacrylic acid (PAA) for 12 hours at room temperature. Synthesis of the PEG–PAA copolymer is performed by mixing polyethylene glycol (PEG) with amine functionality (Surfonamine® L-300) and polyacrylic acid (molecular weight: 5000) (PAA) with a 50% grafting ratio and heating at 120 °C in a nitrogen environment.

### Continuous culture system

The supporting system for running the continuous culture includes the external fluid supplies, pneumatic actuators, optical sensor electronics, temperature controller, and bioreactor control software for controlling oxygen, cell density, and flow rate. The device interface platform consists of a circuit board heater in direct contact with the microfluidic chip and a mounting mechanism to maintain contact and align the chip with the required optical sensors as shown in Fig. 2. The chip output is connected to a thermal electrically cooled 1.5 mL Eppendorf tube for sample collection and chip inputs are connected to pressurized external fluid bottles.

Liquid supply reservoirs were fabricated out of standard GL45 capped glass jars by drilling holes and integrating threaded hose

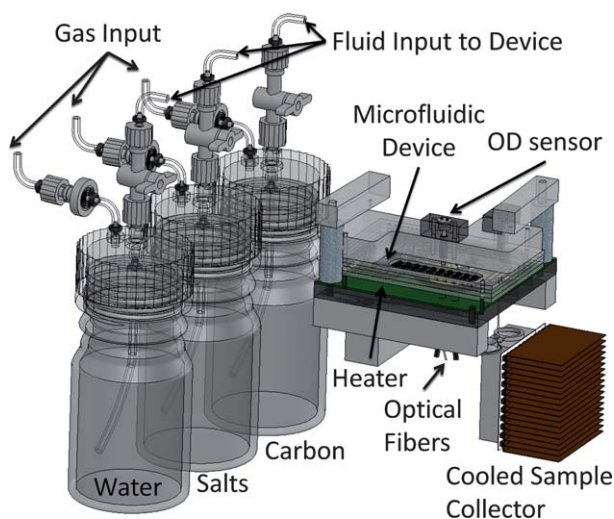


**Fig. 2** Device interface showing the heater, gas and fluid interfaces, mounting mechanism and optical system interface for controlling the microfluidic chip.

barbs for pressure input and fluid output. Fluids were pressurized through 0.22 μm filters (Pall Corporation) and extracted through Tygon tubing (S-50-HL) at the base of each jar. Fluidic interfaces were integrated directly onto the microfluidic chips by machining hose barbs at each fluid input and output.

Pneumatic actuation was performed using miniature 3-way solenoid switches (The Lee Co., LHDA0521111H) driven by digital driver circuits (Freescale MCZ33879). Interfaces for the pressurized gas inputs were also machined directly into each microfluidic device allowing the reuse of a single 20 tube press fit connector.

Optical sensors were addressed by PMMA fiber bundles made from a central 1 mm excitation fiber (Industrial Fiber Optics, IF-C-U1000) and nine surrounding 500 μm collection fibers (IF-C-U500).<sup>4</sup> Excitation fibers were split in the center and placed into a mount allowing integration of color glass filters (CVI Laser, BG3 and BG39). The optical density was measured through a transmission configuration incorporating low numerical aperture optics that permitted a linear correlation between optical density and cell density up to (1 cm OD<sub>600 nm</sub> > 50).

The optical collection fibers terminated at silicon photodetectors connected to transimpedance amplifiers. For oxygen sensors, long pass filters (CVI laser, RG9) were used, and for optical density and pH sensors, shorter wavelength long pass filters were used (KOPP 3482). Plastic mounts allowed integration and alignment of collection fibers, filters, and photodetectors. Photodetectors, transimpedance amplifiers, and analog to digital converters were integrated onto circuit boards for direct digital readout.

Heaters and digital temperature sensors (LM95231) were directly integrated on circuit boards and mounted at the base of each device. All digital control of solenoid drivers, data acquisition, and temperature were performed by a field-programmable gate array (FPGA) (Opal Kelly XEM3100-1500P). System control was performed in MATLAB which measured and processed optical sensor data and ran control loops for oxygen and flow rate.

### Environmental sensors

**Oxygen sensors.** Devices incorporate optical oxygen sensor spots in the base of the growth chamber sections as shown in Fig. 1(b). Dissolved oxygen sensors were fabricated using platinum(II) octaethylporphine-ketone (PtOEPK) embedded in polystyrene and immobilized on glass disks.<sup>20</sup> Sensor spots were calibrated by supplying different ratios of air and nitrogen with regulators and measuring phase. Extracted time constants are similar to other measurements<sup>20</sup> and have been reported previously.<sup>18</sup> No sensor drift was observed for 3 weeks of continuous use and was tested by measuring minimum and maximum phase responses before and after growth experiments. Measurements of oxygen transfer rate were performed through the dynamic gassing method<sup>21</sup> by step changing the mixing gas from helium to air and measuring the time constant for oxygen delivery into the reactor using the optical oxygen sensor.

**pH sensors.** pH sensor spots were purchased from Presens GmbH. While pH sensors were commercially precalibrated, additional calibration of pH sensor phase was performed by

measuring the sensor phase when exposed to buffer solutions varying from pH 5 to pH 10. Due to the potential for pH sensor drift through photobleaching, the medium was offline sampled daily and the pH was referenced to a commercial measurement system (Microelectrodes Inc. MI-410) to ensure accurate online measurements.

**OD sensors.** OD sensors consisted of 590 nm LEDs directly illuminating through the microfluidic device and captured by 500  $\mu\text{m}$  collection fibers located directly under the device. To maintain a fixed volume for optical density measurements, the density was measured in the rigid pass-through channel and the rigid connecting growth chamber channel with path lengths of 850  $\mu\text{m}$  and 116  $\mu\text{m}$  to accommodate different cell densities. For the smaller OD values used for the continuous culture experiment, data from the longer 850  $\mu\text{m}$  path length were used and resulted in an OD resolution of  $\pm 0.013$  and  $\pm 0.02$  OD units at OD = 1 and OD = 2, respectively, due to noise in the measurement electronics. The absolute OD was calibrated by measuring different cell concentrations from the microreactor and comparing to commercial spectrophotometer data (Spectronic 20 Genesys) from concurrent 100  $\mu\text{L}$  output samples. Comparison of online measurements and offline measurements resulted in an accuracy for online OD measurements of  $\pm 0.09$  OD units for differences between online and offline data averaged over 288 hours.

**HPLC analysis.** For HPLC measurements, 50 to 100  $\mu\text{L}$  of the continuous culture output was collected, centrifuged, and frozen immediately. For steady state measurements, HPLC samples were taken after steady state was reached. For dynamic experiments, HPLC samples were taken every 10 minutes by the cooled sample collector, centrifuged, and frozen. HPLC analysis was performed offline on all samples after finishing the continuous culture experiment.

### Control algorithms

**Temperature control.** The temperature was controlled through a closed loop PID controller between the FPGA and the digital temperature sensor mounted at the base of the device. The refresh rate of the controller was 13 Hz and the step response of the closed loop controller was approximately 2 minutes.

**Dissolved oxygen control.** The dissolved oxygen was controlled by varying the oxygen concentration of the growth chamber peristaltic mixer actuation gas. A solenoid valve upstream of the mixer control solenoid valves adjusted the input gas concentration by varying the duty cycle of two input gases, oxygen and helium, at 3 psi. The valve actuation period was set to 10 Hz and alternated between either an oxygen or helium humidification reservoir. The duty cycle of the switch was controlled by a computer which periodically polled the FPGA for optical sensor data at a period of 30 seconds and ran a proportional-integral control algorithm based on the error between the measured oxygen and the oxygen setpoint.

**Flow control.** The flow rate was controlled by the computer system using optical density data measured at a 30 second period.

For turbidostat control, a simple on-off control algorithm was used where the flow rate was set to either a high or low value depending on an optical density threshold. For chemostat control and feed control, the flow rate was set open loop by the software to a programmed injection rate *versus* time profile.

### *Escherichia coli* culture

**Inoculation.** The full deflection mixer allows automatic removal of most of the fluid volume in the growth chamber. To inoculate, one output valve is opened (B4 = O) and all three growth chamber sections are pressurized to remove the internal air and reduce the chamber volume to nearly zero. Then a sterile tube is connected to the output to introduce the inoculum. For inoculation, two of the growth chamber sections are depressurized, allowing them to backfill to 1 mL from the inoculation tube while still preventing the third growth chamber section from filling. The output port is closed to seal the chamber (B4 = P). If any air bubbles exist in the reactor, the inoculation procedure can be repeated indefinitely until all of the internal air bubbles have been removed.

**Cell and medium preparation.** *Escherichia coli* FB21591 (thiC::Tn5-pKD46, Kan<sup>R</sup>), obtained from the *E. coli* Genome Project at the University of Wisconsin (<http://www.genome.wisc.edu>), was used in continuous culture experiments. Inocula for experiments were prepared by streaking LB (Luria-Bertani) plates with 100 mg L<sup>-1</sup> kanamycin from a frozen stock followed by 5 mL test tube growths at 37 °C in LB with 100 mg L<sup>-1</sup> kanamycin. After reaching stationary phase, cells are transferred into 5 mL of defined medium and grown again to stationary phase. A 5 mL inoculum at OD<sub>600 nm</sub> = 0.01 was prepared from the defined medium test tube culture for direct injection into the continuous culture microreactor. Previous measurements of optical density for this cell line resulted in a conversion factor to dry cell weight (dcw) of 0.33 g dcw per L per OD.<sup>4</sup>

The defined medium for test tube cultures<sup>22</sup> consisted of (per litre): 13.5 g KH<sub>2</sub>PO<sub>4</sub>, 4.0 g (NH<sub>4</sub>)<sub>2</sub>HPO<sub>4</sub>, 1.4 g MgSO<sub>4</sub>·H<sub>2</sub>O, 1.7 g citric acid, 0.3 g thiamine, 5 g glucose, 10 mL trace metal solution, and 100 mg kanamycin which were all filter sterilized and stored in an autoclaved glass bottle. The trace metal solution was composed of (per litre 5 M HCl): 10.0 g FeSO<sub>4</sub>·7H<sub>2</sub>O, 2.0 g CaCl<sub>2</sub>, 2.2 g ZnSO<sub>4</sub>·7H<sub>2</sub>O, 0.5 g MnSO<sub>4</sub>·4H<sub>2</sub>O, 1.0 g CuSO<sub>4</sub>·5H<sub>2</sub>O, 0.1 g (NH<sub>4</sub>)<sub>6</sub>Mo<sub>7</sub>O<sub>24</sub>·4H<sub>2</sub>O, and 0.02 g Na<sub>2</sub>B<sub>4</sub>O<sub>7</sub>·10H<sub>2</sub>O.

Defined medium for continuous cultures were split into individual components. The same defined medium specified for test tube cultures but without glucose was placed in one feed bottle. Two other feed bottles were used, one containing DI water and one containing 10 g L<sup>-1</sup> glucose, both of which were steam sterilized in an autoclave.

**Sterilization.** To ensure sterility devices were placed in heat sealed bags and gamma irradiated at 16 kGy. Medium components were mixed and then filter sterilized into autoclaved bottles. Separation of feed bottles into pure chemical components ensured that chemotaxis and feed bottle contamination were prevented since no feed bottle contained enough components to support cell growth and culture media was prepared on-chip. Tests for upstream contamination and growth chamber

contamination were performed at the end of the experiment by streaking the initial culture with the harvested microreactor fluid from before the peristaltic pump and within the growth chamber. Sterility and contamination data are given in the ESI†.

## Results and discussion

### Mixing

Mixing was characterized by measuring the contrast range of images taken with a digital camera (Opteon) for a solution of 0.3 mM bromothymol blue after addition of 0.1 M hydrochloric acid and sodium hydroxide by the peristaltic pump.<sup>23</sup> Single exponential fits to the contrast change *versus* time resulted in a maximum mixing speed of 2 seconds at actuation conditions of 3 psi and 2 Hz full cycle. The mixing speed was highly dependent on the actuation frequency, with a clear maximum efficiency at 2 Hz as shown in Fig. 3. Faster frequencies resulted in incomplete deflection and inefficient turbulent flow generation while slower frequencies resulted in full deflection faster than the actuation frequency and substantial wait time between states.

Fast homogenous mixing was possible by forcing fluid through small channels located between the mixer sections and by allowing full vertical deflection of the chamber from 0 mm to 2 mm forcing a large volume displacement with each stroke. A movie illustrating the mixing pattern is provided in the ESI†.

### Oxygen transfer coefficient

Unlike previously fabricated all PDMS devices,<sup>4</sup> oxygen transfer rates in plastic devices are not complicated by multiple paths for

oxygen diffusion. In addition, the mixing times are fast enough to approximate as instantaneous in comparison with the oxygen diffusion time. The differential equation governing oxygen diffusion into the reactor assumes perfect fluid mixing since the concentration of dissolved oxygen,  $C$ , is not a function of position.

$$\frac{\partial C}{\partial t} = K_L a (C_{in}(t) - C) - OUR \quad (1)$$

where  $k_L a$  is the oxygen transfer rate of the system, including diffusion through the PDMS, surface area of PDMS–water contact, and water volume,  $C_{in}$  is the saturation concentration in the liquid for a given oxygen partial pressure, and OUR is the oxygen uptake rate. For a one dimensional diffusion system with instantaneous mixing, this differential equation accurately describes the dynamics of oxygen in the liquid. Therefore, established methods for measuring  $k_L a$  such as the dynamic gassing method<sup>21</sup> can be used to characterize the reactor.

Dynamic gassing measurements in Fig. 4 show a maximum  $k_L a$  of 0.016  $s^{-1}$  and 0.025  $s^{-1}$  for input pressures of 3 psi and 7 psi respectively. Since the membranes are capable of laminating both the upper and lower surfaces of the growth chamber, resulting in a decrease in the contact area between the PDMS and the gas headspace, a pressure dependence of  $k_L a$  is expected.

Since  $k_L a$  determines the maximum supported cell density in the reactor, it can be used to calculate the maximum OD supported by the system. Setting eqn (1) to steady state and assuming that the concentration of dissolved oxygen in the water is zero, we calculate the maximum cell density supported to be OD = 14.7, assuming  $C_{in} = 1.26 \text{ mM}$ <sup>24</sup> for a maximum water solubility of pure oxygen at 37 °C and 3 psi, a maximum

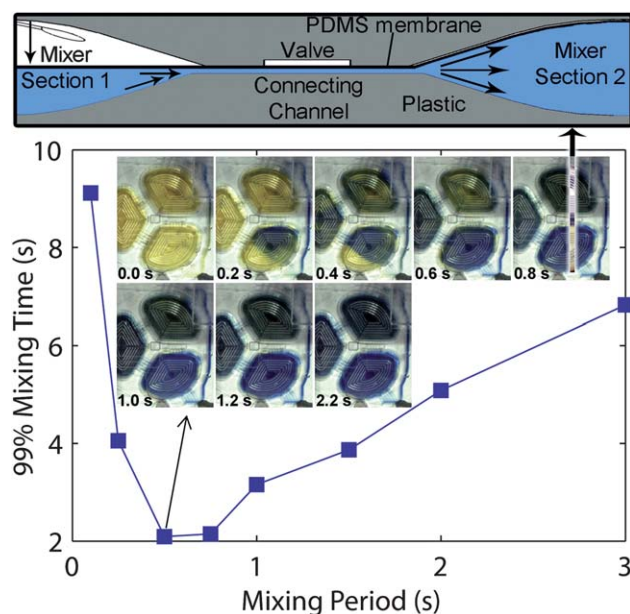


**Fig. 3** (Top) Schematic of the mixing cross-section between two growth chamber sections. When one section is pressurized and inflated, fluid is pushed through a connecting channel, forcing the low pressure sections to deflate and fill with liquid. (Bottom) Mixing efficiency for the full deflection membrane mixer. Mixing times of 2 seconds are achievable at mixing periods of 500 ms. (Inset) Time course for mixing from acidic to basic conditions at a mixing period of 500 ms.

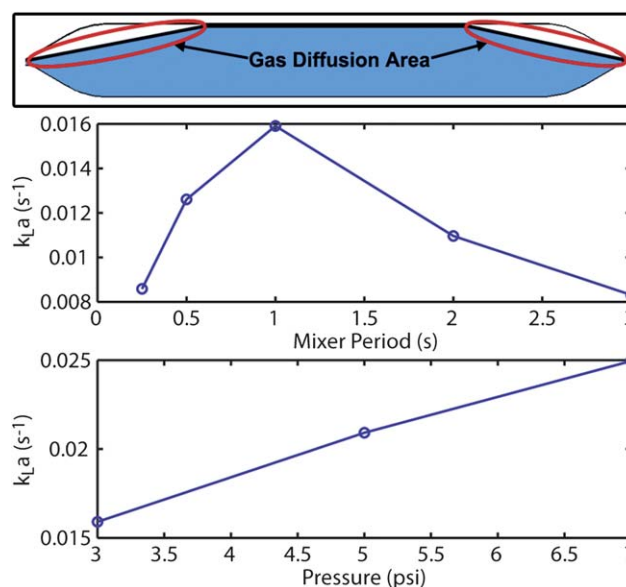


**Fig. 4** Dependence of the mixer oxygen transfer rate ( $k_L a$ ) on the mixer parameters of period and pressure. (Top) Oxygen transfer rate depends on both parameters due to their affect on the available area for gas to liquid diffusion. As shown in the schematic, the diffusion area changes as the PDMS membrane inflates into the upper wall of the chamber. (Middle) Optimum oxygen transfer occurs at a mixer period of 1 second. (Bottom) Oxygen transfer rate improves as the pressure increases.

OUR = 15.4 mmol O<sub>2</sub> per g dcw per h,<sup>25</sup> 0.33 g dcw per L per OD, and a  $k_{LA} = 0.016 \text{ s}^{-1}$ . Previously reported continuous culture systems did not require growth beyond OD = 7.5<sup>6,8,26,27</sup> suggesting that the system is adequate for continuous culture experiments.

### Flow rate

The flow rate through the peristaltic pump was characterized by attaching a capillary tube to the output of the device. A measurement system utilizing a triggered CCD camera (Opteon) and a 600  $\mu\text{m}$  inner diameter glass capillary (McMaster 8729K57) tube was used, resulting in a volume resolution of 18 nL per pixel. An image was captured every pump period and processed in MATLAB to determine the position of the meniscus. Details of the measurement are given in the ESI†.

The flow rate through the peristaltic pump was characterized for various backpressures from the external fluid input. As shown in Fig. 5, the volume varies by nearly a factor of two for input pressure variations from 0 to 3 psi. Enabling the on-chip reservoir with a 1.5 psi pressure at the reservoir pressure input effectively eliminates these variations and maintains a consistent injection volume of 200 nL over the 3 psi range in external fluid pressure.

### *E. coli* continuous culture

A 3 week long continuous culture experiment was performed using the bioreactor to demonstrate device operation and novel control conditions possible with the device which enable direct observation of cell metabolic processes. Since glucose and salts were separated into individual feed bottles, the peristaltic pump

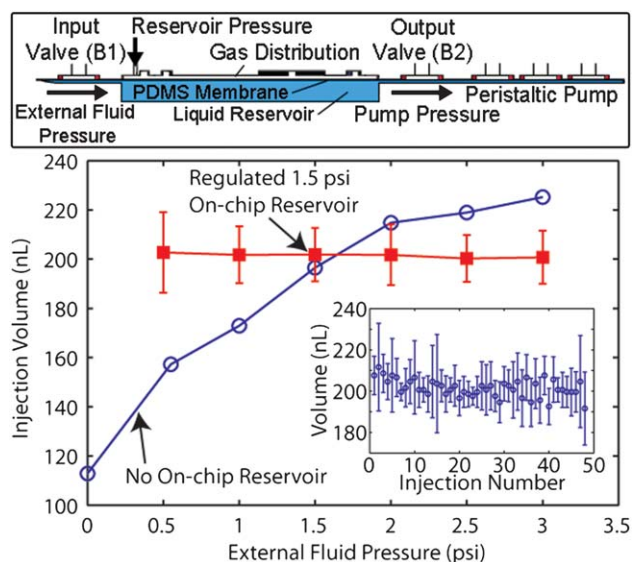


**Fig. 5** (Top) Cross-section schematic of the on-chip pressure regulator. The external fluid reservoirs provide driving pressure into the device while the reservoir pressure and gating valves B1 and B2 provide a regulated pump pressure. (Bottom) Comparison of injection volume versus external fluid pressure with and without an on-chip reservoir pressurized at 1.5 psi. (Inset) Injection volume versus injection number averaged over all regulated external fluid pressure conditions.

could vary the concentration of glucose in the feed. The glucose concentration was adjusted by changing the ratio of DI water to glucose injections while keeping the total injections equal to the salt injections. This prevented dilution of the salt media. Due to the ability to switch between multiple inputs and accurately measure the optical density, pH, and oxygen, a variety of new functions are now possible. Multiple experiments in chemostat and turbidostat modes with different media compositions can be run in a single device, modulation of input sources are possible, HPLC sample collection times are fast enough to look at dynamics, control of oxygen during continuous culture can now be implemented, and operation for 3 weeks without evaporation is possible, all while maintaining sterility. Online growth data from the continuous culture are given in Fig. 6.

Initially, the cells are grown in batch to assess the viability and oxygen transfer as shown in Fig. 6(a). This results in a significant decrease in pH typical of batch growths. Even at OD 4, the oxygen supply was sufficient to maintain an oxygen concentration of 50% air saturation. Then continuous culture is turned on to observe known *E. coli* metabolic functions. Chemostat operation is initiated at flow rates specified in the flow rate plot and the corresponding cell densities are given in Fig. 6(b). Consistent with previous continuous culture experiments,<sup>28</sup> increase in the flow rate at 50 hours results in higher optical density at the same glucose concentration.

At 120 hours in Fig. 6(c), the flow rate is ramped up to induce washout. This allows us to sweep the flow rate to approximately

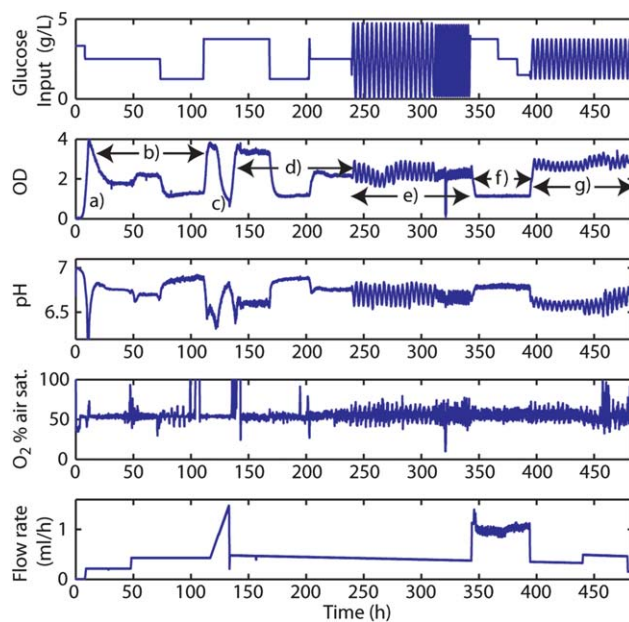


**Fig. 6** Data from the second continuous culture experiment using *E. coli* FB21591. Different steady states and dynamic states based on glucose control are demonstrated in both chemostat and turbidostat modes. (a) Cells are grown in batch before initiating continuous flow. (b) Chemostat operation at different flow rates and glucose concentrations. (c) Washout conditions. (d) Repeated chemostat operation at different glucose concentrations. (e) Chemostat operation at dynamically varying glucose concentrations. (f) Turbidostat operation at different glucose concentrations. (g) Dynamically varying glucose concentrations in a chemostat at different flow rates.

find the maximum growth rate. If we estimate the maximum growth rate as when the cell density starts to decrease, we get a maximum growth rate of  $0.85 \text{ h}^{-1}$ . From HPLC sampling during washout given in Fig. 7(a), we also see acetic acid and glucose accumulation when the cell density starts to decrease, typical of overflow metabolism.<sup>25</sup> Restoration of chemostat operation at 155 hours results in complete removal of glucose and acetate from the medium as expected.

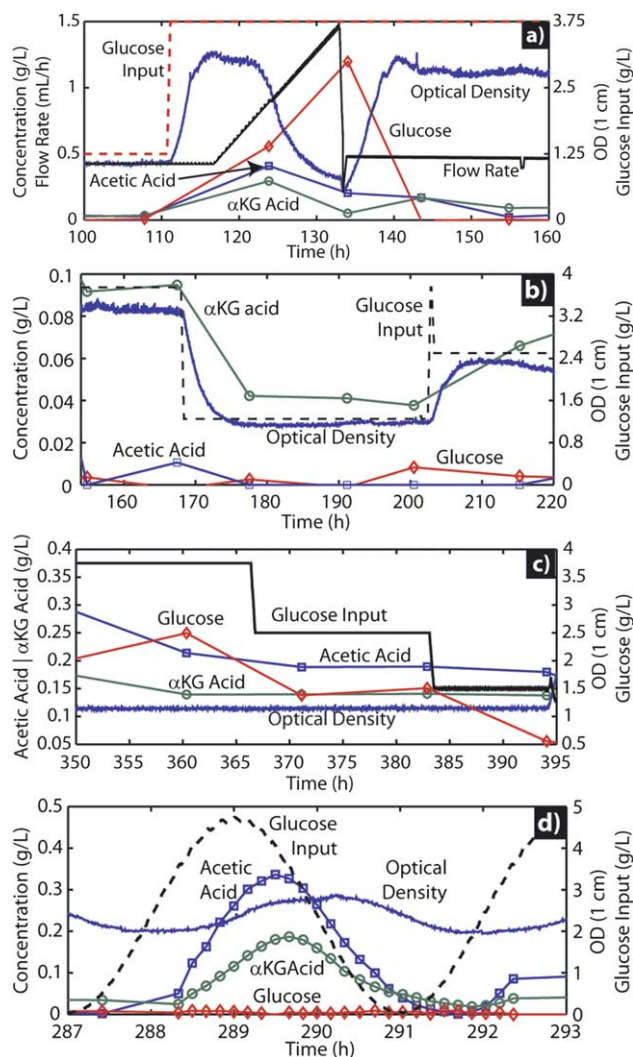


**Fig. 7** HPLC analysis from three different operation modes in the continuous reactor. (a) After establishing chemostat steady state, the flow rate is ramped to induce washout. This results in glucose accumulation and acetic acid production with an accompanying decrease in cell density. (b) Chemostat steady state is shown with the ability to control cell density by varying the glucose concentration. In addition to cell density being proportional to glucose concentration,  $\alpha$ -ketoglutaric acid is also proportional, suggesting a constant rate of respiration for the given growth rate. (c) Turbidostat steady state is demonstrated. By maintaining a constant cell density and maximum growth, increases in glucose concentration allow direct observation of increased acetate production due to overflow metabolism.  $\alpha$ -Ketoglutaric acid production is also increased suggesting higher metabolic activity associated with the faster growth rate. (d) Demonstration of sinusoidal modulation of input glucose and resulting acid dynamics measured with HPLC.

After washout, three steady states at different input glucose concentrations demonstrate that the cell density can be controlled by changing the glucose concentration as shown in Fig. 6(d). The cells grow in direct proportion to the glucose input as expected for chemostat operation, with optical densities of  $1.16 \pm 0.024$ ,  $2.22 \pm 0.074$ , and  $3.33 \pm 0.040$  for input glucose concentrations of  $1.25 \text{ g L}^{-1}$ ,  $2.5 \text{ g L}^{-1}$ , and  $3.75 \text{ g L}^{-1}$  respectively. Looking at the HPLC data in Fig. 7(b), we see that in chemostat operation, the acid production is very different from what we see in washout conditions. Instead of the cells producing acetic acid, the majority of acid production is  $\alpha$ -ketoglutaric acid and succinic acid. Since the quantities of each track almost identically throughout the growth, only  $\alpha$ KG acid is shown. The production of  $\alpha$ KG acid is also proportional to the cell density, with an average production rate of  $0.042 \pm 0.005 \text{ g per g dcw per h}$  suggesting that the production rate per cell is not actually changing with glucose input. Chemostat experiments using feed control demonstrate the ability to control the cell density online by varying the glucose concentration.

In contrast to chemostat operation, turbidostat operation allows one to study the metabolic behavior of cells in washout conditions such as overflow metabolism and maximum growth rate in steady state. Turbidostat operation is shown in Fig. 6(f). Cells are maintained at an OD of  $1.14 \pm 0.013$ , demonstrating closed loop control of OD to within 1.2%. Looking at the flow control variable, we can extract a maximum growth rate of  $0.994 \pm 0.051 \text{ h}^{-1}$ . This value is higher than estimations from washout, demonstrating that washout underestimates the maximum cell growth rate. In addition to flow control, since we can change the glucose input concentration without affecting the flow rate, we can observe overflow metabolism directly. From the HPLC data shown in Fig. 7(c) during turbidostat operation, we can see that acetate production increases as the glucose concentration in the reactor increases as expected.<sup>25</sup>  $\alpha$ -Ketoglutaric acid production, which was proportional to the cell density in chemostat operation, also does not change in turbidostat operation at constant OD. However, the amount of acid produced is higher at  $0.368 \pm 0.026 \text{ g per g dcw per h}$ . This could reflect an increase in cell metabolism and the citric acid cycle during turbidostat operation.

While steady state operation allows the potential to probe cell metabolism through mass balances, dynamic operation can also enable probing of how cells respond dynamically to changes in input concentrations. As shown in Fig. 6(e) and (g), individual component control at the input allows for programmed input dynamics such as sinusoidal modulation of glucose at different frequencies. This type of operation could be used to study time responses of different metabolic pathways. Since the reactor volume is 1 mL, high speed sampling for HPLC analysis can also be performed, resulting in high resolution data of the chemical responses to input feed modulation as shown in Fig. 7(d).

## Conclusions

This work has demonstrated long term microscale continuous culture of *E. coli* for 500 hours. By developing a device platform that incorporates rigid materials with PDMS membranes, a novel strategy for evaporation prevention and reliable flow control is demonstrated allowing long term operation without

concentration drift. An integrated peristaltic pump enables online flow control and multiple inputs allow on-chip media preparation and concentration control. Both cell density control in chemostat mode using glucose and cell density control in turbidostat mode using flow rate are demonstrated.

By operating with a larger 1 mL volume in comparison with previous devices, HPLC analysis of chemical concentrations in the different steady state and dynamic states of operation is possible enabling detailed observation of cell metabolism. From chemostat experiments, steady state production of different acids or products can be characterized. From turbidostat experiments, maximum cell growth rates can be directly measured and observation of overflow metabolism can be analyzed to determine acid yields. Finally, the potential for dynamic concentration and flow control allows for more complex input waveforms which can be used to characterize cell dynamics or induce chemically dependent responses. Such experiments would be important for characterizing biological behavior such as genetic switches, environmental shock responses, directed evolution, co-metabolism, and co-culture dynamics.

### Acknowledgements

We would like to thank Professor Kristala Jones Prather and Diana Bower for providing HPLC analysis and the National Science Foundation for funding this work.

### References

- 1 J. Monod, *Ann. Inst. Pasteur (Paris)*, 1950, **79**, 390–410.
- 2 A. Novick and L. Szilard, *Science*, 1950, **112**, 715–716.
- 3 P. A. Hoskisson and G. Hobbs, *Microbiology*, 2005, **151**, 3153–3159.
- 4 H. L. T. Lee, P. Boccazzi, R. J. Ram and A. J. Sinskey, *Lab Chip*, 2006, **6**, 1229–1235.
- 5 F. K. Balagadde, L. You, C. L. Hansen, C. L. Arnold and S. R. Quake, *Science*, 2005, **309**, 137–140.
- 6 Z. Zhang, P. Boccazzi, H. G. Choi, G. Perozziello, A. J. Sinskey and K. F. Jensen, *Lab Chip*, 2006, **6**, 906–913.
- 7 X. Luo, K. Shen, C. Luo, H. Ji, Q. Ouyang and Y. Chen, *Biomed. Microdevices*, 2010, **12**, 499–503.
- 8 A. Edlich, V. Magdanz, D. Rasch, S. Demming, S. A. Zadeh, R. Segura, C. Kahler, R. Radespiel, S. Buttgenbach, E. Franco-Lara and R. Krull, *Biotechnol. Prog.*, 2010, **26**, 1259–1270.
- 9 A. Groisman, C. Lobo, H. Cho, J. K. Campbell, Y. S. Dufour, A. M. Stevens and A. Levchenko, *Nat. Methods*, 2005, **2**, 685–689.
- 10 J. Flegr, *J. Theor. Biol.*, 1997, **188**, 121–126.
- 11 V. Bryson and W. Szybalski, *Science*, 1952, **116**, 43–51.
- 12 E. Blumwald and E. Tel-Or, *Plant Physiol.*, 1984, **74**, 183–185.
- 13 J. H. Slater and I. Morris, *Arch. Mikrobiol.*, 1973, **92**, 235–244.
- 14 C. C. Parrish and P. J. Wangersky, *Mar. Ecol.: Prog. Ser.*, 1987, **35**, 119–128.
- 15 J. C. Gottschal and J. G. Morris, *Biotechnol. Lett.*, 1982, **4**, 477–482.
- 16 K. S. Lee and R. J. Ram, *Lab Chip*, 2009, **9**, 1618–1624.
- 17 M. A. Unger, H. P. Chou, T. Thorsen, A. Scherer and S. R. Quake, *Science*, 2000, **7**, 113–116.
- 18 K. S. Lee, H. L. T. Lee and R. J. Ram, *Lab Chip*, 2007, **7**, 1539–1545.
- 19 W. V. Sorin and D. F. Gray, *IEEE Photonics Technol. Lett.*, 1992, **4**, 105–107.
- 20 D. B. Papkovsky, G. V. Ponomarev, W. Trettnak and P. O'Leary, *Anal. Chem.*, 1995, **67**, 4112–4117.
- 21 V. Linek, P. Benes and V. Vacek, *Chem. Eng. Technol.*, 1989, **12**, 213–217.
- 22 F. Wang and S. Y. Lee, *Biotechnol. Bioeng.*, 1998, **58**, 325–328.
- 23 N. Szita, P. Boccazzi, Z. Zhang, P. Boyle, A. J. Sinskey and K. F. Jensen, *Lab Chip*, 2005, **5**, 819–826.
- 24 C. N. Murray and J. P. Riley, *Deep-Sea Res. Oceanogr. Abstr.*, 1969, **16**, 311–320.
- 25 B. Xu, M. Jahic and S. Enfors, *Biotechnol. Prog.*, 1999, **15**, 81–90.
- 26 E. M. T. El-Mansi and W. H. Holms, *J. Gen. Microbiol.*, 1989, **135**, 2875–2883.
- 27 S. J. Berrios-Rivera, G. N. Bennet and K. Y. San, *Metab. Eng.*, 2002, **4**, 230–237.
- 28 A. Kayser, J. Weber, V. Hecht and U. Rinas, *Microbiology*, 2005, **151**, 693–706.